

Constrained Stein Variational Trajectory Optimization

Thomas Power¹ and Dmitry Berenson¹

Abstract—We present Constrained Stein Variational Trajectory Optimization (CSVTO), an algorithm for performing trajectory optimization with constraints on a set of trajectories in parallel. We frame constrained trajectory optimization as a novel form of constrained functional minimization over trajectory distributions, which avoids treating the constraints as a penalty in the objective and allows us to generate diverse sets of constraint-satisfying trajectories. Our method uses Stein Variational Gradient Descent (SVGD) to find a set of particles that approximates a distribution over low-cost trajectories while obeying constraints. CSVTO is applicable to problems with arbitrary equality and inequality constraints and includes a novel particle resampling step to escape local minima. By explicitly generating diverse sets of trajectories, CSVTO is better able to avoid poor local minima and is more robust to initialization. We demonstrate that CSVTO outperforms baselines in challenging highly-constrained tasks, such as a 7DoF wrench manipulation task, where CSVTO succeeds in 20/20 trials vs 13/20 for the closest baseline. Our results demonstrate that generating diverse constraint-satisfying trajectories improves robustness to disturbances and initialization over baselines.

I. INTRODUCTION

Trajectory optimization and optimal control are powerful tools for synthesizing complex robot behavior using appropriate cost functions and constraints [1]–[5]. Constraint satisfaction is important for safety-critical applications, such as autonomous driving, where constraints determine which trajectories are safe. Constraints can also provide effective descriptions of desired behavior. For instance, consider a robot sanding a table. This problem can be defined with an equality constraint specifying that the end-effector must move along the surface of the table as well as constraints on the minimum and maximum force applied to the table. For many tasks, including manipulation tasks like the one above, satisfying these constraints can be very difficult as constraint-satisfying trajectories may lie on implicitly defined lower-dimensional manifolds. This is an issue for sample-based methods since the feasible set has zero measure and thus it is difficult to sample. It is also difficult for gradient-based methods since even for trajectories that start feasible, if the constraint is highly nonlinear then updates based on a first-order approximation of the constraint will lead to solutions leaving the constraint manifold. In addition, many useful tasks entail constrained optimization problems that are non-convex and exhibit multiple local minima.

One of the key advantages of trajectory optimization techniques over global search methods, such as sampling-based motion planning, is computational speed. This can enable fast online re-planning to adapt to disturbances. For example, consider again the robot sanding the table, but now in the

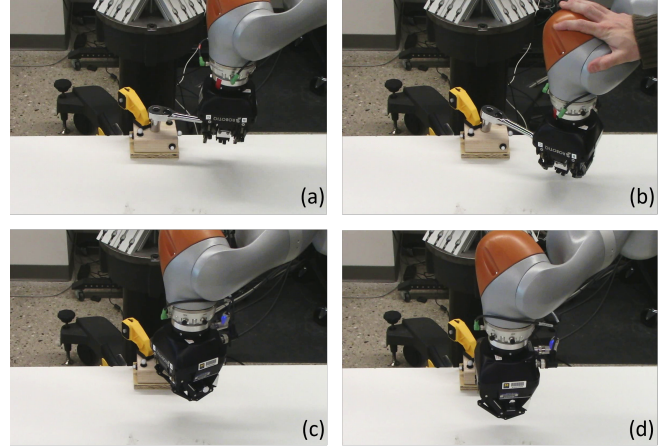


Fig. 1. We use CSVTO to turn a wrench in the real world with online replanning; b) A human disturbs the robot, changing the grasp position of the wrench; c) The robot readjusts the grasp position; d) The robot achieves the desired wrench angle.

proximity of a human. The human may move in an unexpected way which necessitates an update to the planned trajectory. However, the performance of many trajectory optimization methods is highly dependent on the initialization. Poor initialization may lead to highly sub-optimal, or even infeasible solutions. This is particularly problematic when re-solving the optimization problem online under limited computation time when disturbances can lead to the previous solution becoming a poor initialization for the current optimization problem. In the example above, the human may move to block the robot's path, and performing a local optimization starting from the previous trajectory may not return a feasible solution.

In this article, we formulate the constrained trajectory optimization problem as a Bayesian inference problem. This view has advantages as it aims to find a distribution over trajectories rather than a single trajectory alone. As noted by Lambert et. al. [6], commonly used Variational Inference approaches [7] lead to minimizing entropy-regularized objectives [6] which can improve exploration of the search space and give greater robustness to initialization. Previous methods taking the inference view of trajectory optimization have only been able to incorporate constraints via penalties in the cost [6], [8]–[10]. A drawback of penalty methods is that selecting the relative weights of the penalties is challenging due to possible conflicts with the objective. We compare against baselines that incorporate constraints via penalties and show that, for non-trivial constraints, this results in poor constraint satisfaction.

We propose Constrained Stein Variational Trajectory Optimization (CSVTO), an algorithm that uses a non-parametric approximation of the posterior over low-cost constraint-

This work was sponsored by Honda Research Institute USA. ¹Authors are with the Robotics Department, University of Michigan, Ann Arbor, MI, USA. {tpower, dmitryb}@umich.edu

satisfying trajectories. Our method builds on Orthogonal-Space Stein Variational Gradient Descent (O-SVGD), a recent non-parametric variational inference method for domains with a single equality constraint [11]. We present a constrained SVGD algorithm for trajectory optimization which is able to handle arbitrary equality and inequality constraints. Our method performs a constrained optimization on a set of trajectory particles, resulting in a diverse set of approximately constraint-satisfying trajectories. We additionally incorporate a novel resampling step that resamples and perturbs particles in the tangent-space of the constraints to escape local minima. Our contributions are as follows:

- We frame constrained trajectory optimization as a novel form of constrained functional minimization over trajectory distributions, which avoids treating the constraints as a penalty in the objective.
- We present a constrained SVGD algorithm for trajectory optimization, which is applicable to problems with arbitrary twice differentiable equality and inequality constraints.
- We propose a novel particle resampling step for resampling and perturbing trajectory particles in the tangent-space of the constraints to escape local minima.
- We evaluate our method on three complex constrained problems, including a 12DoF underactuated quadrotor and two highly constrained 7DoF manipulation tasks.

Our experimental results demonstrate that CSVTO is able to outperform baselines in challenging, highly constrained tasks, such as a 7DoF wrench manipulation task where our method achieves 20/20 success compared with 13/20 for IPOPT [12] and 12/20 for SVMPC [10]. In addition, CSVTO outperforms baselines in a 12DoF quadrotor task with a dynamic obstacle that necessitates online adaption of the planned trajectory.

The article is organized as follows. In Section II we discuss related work. In Section III we will discuss the trajectory optimization problem, followed by an overview of the variational inference approach to trajectory optimization in Section IV. In Section V we introduce our novel formulation of trajectory optimization as a constrained functional minimization over trajectory distributions. We will then give some additional background information on SVGD in Section VI which is necessary to develop our algorithm. In Section VII we introduce CSVTO. In Section VIII we evaluate our method on a 12DoF quadrotor task and two highly constrained tasks with a 7DoF manipulator. We additionally deployed CSVTO to turn a wrench in the real world (Figure 1).

II. RELATED WORK

A. Trajectory optimization

Previous work on local trajectory optimization techniques includes direct methods [4], [13], where the explicit optimization problem is transcribed and solved using nonlinear solvers such as IPOPT [12] or SNOPT [14]. Methods in this class include Sequential Convex Programming (SCP) methods such as TrajOpt [2] and GuSTO [1], as well as barrier methods [15], [16]. In contrast, indirect methods aim instead to solve the local optimality conditions of the trajectory and early

examples include DDP [17] and ILQR [18], however, neither of these methods can handle constraints. Later work incorporated constraint satisfaction with these indirect methods [3], [19], [20]. Direct methods are typically easier to initialize but less accurate [21]. However all of these methods only aim to find a single locally-optimal trajectory, and the performance is dependent on the initialization. In contrast, our approach optimizes a diverse set of trajectories in parallel. This makes our approach easier to initialize as well as more robust to disturbances when re-planning online. Our approach is related to the direct methods, in that we use an iterative algorithm that aims to minimize an objective. However, our method is based on viewing the trajectory optimization problem as a Bayesian inference problem.

B. Sample-based Motion Planning

Many global search methods have been developed in the sampling-based motion planning literature, yielding motion planners for constrained domains. These can be broadly categorized as projection methods, whereby sampled configurations are projected to the constraint [22], [23], and continuation methods, which use a local approximation of the constraint manifold at feasible configurations to sample new configurations [24], [25]. Our method of trajectory optimization is similar to continuation methods, as our iterative algorithm projects update steps to the tangent space of the constraint. While these global motion planners can be highly effective, they are typically too computationally intensive to be run online.

C. Planning & Control as Inference

Prior work framing trajectory optimization as Bayesian inference has used Gaussian approximations to yield fast, gradient-based algorithms [8], [9], [26]–[29]. Sample-based techniques such as MPPI [30] and CEM [31] have strong connections to the inference formulation of Stochastic Optimal Control (SOC) [32], but these methods again use Gaussian sampling distributions. Watson and Peters recently proposed using a Gaussian Process as a sampling distribution [33], resulting in smoother trajectories. However, the resulting sampling distribution is still Gaussian. Gaussian sampling distributions can be problematic in complex environments due to their lack of flexibility which hinders exploration of the search space. Recent work has proposed learning non-Gaussian sampling distributions with flexible model classes [34], [35].

Another class of methods has used Stein Variational Gradient Descent (SVGD) [36] for MPC [10], [37] and trajectory optimization [6]. By using particle approximations these methods can generate multi-modal trajectory distributions. SVGD has also been used to improve Probabilistic Roadmaps (PRMs) [38]. Our method is also based on SVGD.

However, to date, control-as-inference-based methods have been unable to handle highly constrained domains. Recently CCSMPPI [39] was proposed which can satisfy chance inequality constraints, but is restricted to linear systems. Our method uses SVGD to generate diverse sets of *constraint-satisfying* trajectories which can satisfy both inequality and equality constraints. Another method closely related to ours is SMT0

[40], this method treats the trajectory optimization problem as a density estimation problem and alternates between sampling and performing a gradient-based optimization to generate multiple low-cost trajectories that satisfy the constraints. SMTO uses CHOMP [41] to perform the gradient-based optimization sequentially for each sampled trajectory. Our contribution is complementary to SMTO; SMTO could substitute CHOMP with our method, CSVTO, in the gradient-optimization step. This would have the advantage of performing the gradient-based optimization in parallel and encouraging diversity among trajectories.

D. Gradient Flows for constrained optimization

Our method is closely related to methods using gradient flows for constrained optimization. Gradient flows are an optimization method that re-frames optimization as the solution to an ordinary differential equation (ODE); gradient flows can be thought of as continuous-time versions of gradient descent algorithms. Yamashita proposed a gradient flow method for equality-constrained problems [42]. The most common method of extending this to problems with inequality constrained is via the introduction of slack variables to convert inequality constraints to equality constraints [43]–[45]. Our method, CSVTO, also uses slack variables to transform inequality constraints into equality constraints. Recently, Feppon et. al. [46] proposed a method that instead solves a Quadratic Program (QP) subproblem to identify active inequality constraints which are treated as equality constraints in the gradient flow. Jongen and Stein applied constrained gradient flows to global optimization, by proposing a gradient flow algorithm that iterates between searching for local minima and local maxima [45].

SVGD has been interpreted as a gradient flow [47], and similar ideas to those developed in the gradient flows for constrained optimization literature were recently explored in O-SVGD [11]. O-SVGD performs SVGD in domains with a single equality constraint. We extend and modify O-SVGD to domains with arbitrary equality and inequality constraints.

III. TRAJECTORY OPTIMIZATION

Trajectory optimization is commonly modeled as an Optimal Control Problem (OCP). We consider a discrete-time system with state $\mathbf{x} \in \mathbb{R}^{d_x}$ and control $\mathbf{u} \in \mathbb{R}^{d_u}$ and dynamics $\mathbf{x}_t = f(\mathbf{x}_{t-1}, \mathbf{u}_{t-1})$. We define finite horizon trajectories with horizon T as $\tau = (\mathbf{X}, \mathbf{U})$, where $\mathbf{X} = \{\mathbf{x}_1, \dots, \mathbf{x}_T\}$ and $\mathbf{U} = \{\mathbf{u}_0, \dots, \mathbf{u}_{T-1}\}$. Given an initial state \mathbf{x}_0 , the aim when solving an OCP is to find a trajectory τ that minimizes a given cost function C subject to equality and inequality constraints:

$$\begin{aligned} & \min_{\tau} C(\tau) \\ & \text{s.t.} \\ & h(\tau) = 0 \\ & g(\tau) \leq 0 \\ & \forall t \in \{1, \dots, T\} \\ & f(\mathbf{x}_{t-1}, \mathbf{u}_{t-1}) = \mathbf{x}_t \\ & \mathbf{u}_{\min} \leq \mathbf{u}_{t-1} \leq \mathbf{u}_{\max} \\ & \mathbf{x}_{\min} \leq \mathbf{x}_{t-1} \leq \mathbf{x}_{\max}. \end{aligned} \quad (1)$$

Here we have separated general inequality constraints g from simple bounds constraints, as well as the dynamics constraints from other equality constraints h . We additionally assume that C is non-negative and once differentiable and that f, g, h are all twice differentiable. This problem will be non-convex in general, therefore it is likely that the optimization problem in (1) will have multiple local minima. The quality of solutions for most methods for solving this optimal control problem depends heavily on the initialization; often a poor initialization can lead to infeasibility.

IV. VARIATIONAL INFERENCE FOR TRAJECTORY OPTIMIZATION

In this section, we will demonstrate how unconstrained trajectory optimization can be framed as an inference problem, as in [10], [28], [48], [49]. This framing results in estimating a distribution over low-cost trajectories, rather than a single optimal trajectory. By using this framing we can leverage approximate inference tools for trajectory optimization, in particular, Variational Inference [7]. In this section, we will show how this framing leads to an entropy-regularized objective [6] which aims to find a distribution over low-cost trajectories while maximizing entropy. By using an entropy-regularized objective we aim to have improved exploration of the search space and greater robustness to initialization.

To reframe trajectory optimization as probabilistic inference, we first introduce an auxiliary binary random variable o for a trajectory such that

$$p(o = 1|\tau) = \exp(-C(\tau)) \quad (2)$$

which defines a valid probability distribution over o provided C is non-negative. We can trivially see that the trajectory that maximizes the likelihood of $p(o = 1|\tau)$ is the trajectory that minimizes the cost. Introducing this binary variable thus allows us to express the cost as a likelihood function, which we will use in the Bayesian inference formulation of trajectory optimization.

We aim to find the posterior distribution $p(\tau|o = 1) \propto p(o = 1|\tau)p(\tau)$, where $\tau, p(\tau) = p(\mathbf{X}, \mathbf{U})$ is a prior on trajectories. For deterministic dynamics, this prior is determined by placing a prior on controls \mathbf{U} . This prior is a design choice and can be used to regularize the controls. For instance, a squared control cost can be equivalently expressed as a Gaussian prior. Alternatively, this prior could be learned from a dataset of low-cost trajectories [50]. The trajectory prior is

$$p(\tau) = p(\mathbf{U}) \prod_{t=1}^T \delta(\mathbf{x}_t - \hat{\mathbf{x}}_t) \quad (3)$$

where $\hat{\mathbf{x}}_t = f(\mathbf{x}_{t-1}, \mathbf{u}_{t-1})$, and δ is the Dirac delta function. This inference problem can be performed exactly for the case of linear dynamics and quadratic costs [29], [51]. However, in general, this problem is intractable and approximate inference techniques must be used. We use variational inference to approximate $p(\tau|o = 1)$ with distribution $q(\tau)$ which minimizes

the divergence $\mathcal{KL}(q(\tau)||p(\tau|o=1))$ [7]. The quantity to be minimized is

$$\begin{aligned} \mathcal{KL}(q(\tau)||p(\tau|o=1)) &= \int q(\tau) \log \frac{q(\tau)}{p(\tau|o=1)} d\tau \\ &= \int q(\tau) \log \frac{q(\tau)p(o=1)}{p(o=1|p(\tau))} d\tau \end{aligned} \quad (4)$$

$p(o=1)$ does not depend on τ so can be dropped from the minimization. This results in the *variational free energy* \mathcal{F}

$$\mathcal{F}(q) = \int q(\tau) \log \frac{q(\tau)}{p(o=1|\tau)p(\tau)} d\tau \quad (5)$$

$$= -\mathbb{E}_{q(\tau)}[\log p(o=1|\tau) + \log p(\tau)] - \mathcal{H}(q(\tau)) \quad (6)$$

$$= \mathbb{E}_{q(\tau)}[C(\tau)] - \mathbb{E}_{q(\tau)}[\log p(\tau)] - \mathcal{H}(q(\tau)) \quad (7)$$

where $\mathcal{H}(q(\tau))$ is the entropy of $q(\tau)$. Intuitively, we can understand that the first term promotes low-cost trajectories, the second is a regularization on the trajectory, and the entropy term prevents the variational posterior from collapsing to a *maximum a posteriori* (MAP) solution. We may choose to provide regularization on the controls as part of C , in which case the prior term is absorbed into the cost term.

V. PROBLEM STATEMENT

In this article, we frame the constrained optimal control problem introduced in Section III as a probabilistic inference problem, using ideas developed in Section IV.

It is first instructive to consider the dynamics constraint, which is incorporated into the prior in equation (3) via the Dirac delta function. In this case, the term $\mathbb{E}_{q(\tau)}[-\log p(\tau)]$ is infinite for any τ which does not obey the dynamics constraint. We can convert this unconstrained optimization problem with infinite cost to the following constrained optimization problem on the space of probability distributions:

$$\begin{aligned} \min_q \quad & \tilde{\mathcal{F}}(q) \\ \text{s.t.} \quad & \\ & \forall t \in \{1, \dots, T\} \\ & P_q(f(\mathbf{x}_{t-1}, \mathbf{u}_{t-1}) = \mathbf{x}_t) = 1 \end{aligned} \quad (8)$$

where $\tilde{\mathcal{F}}(q)$ is the free energy from equation (7) with the infinite cost term $\sum_{t=1}^T \log \delta(\mathbf{x}_t - f(\mathbf{x}_{t-1}, \mathbf{u}_{t-1}))$ dropped from $\log p(\tau)$, and $P_q(A)$ is the probability of event A under probability measure $q(\tau)$. Applying this process to other constraints we have

$$\begin{aligned} \min_q \quad & \tilde{\mathcal{F}}(q) \\ \text{s.t.} \quad & \\ & P_q(h(\tau) = 0) = 1 \\ & P_q(g(\tau) \leq 0) = 1 \\ & \forall t \in \{1, \dots, T\} \\ & P_q(f(\mathbf{x}_{t-1}, \mathbf{u}_{t-1}) = \mathbf{x}_t) = 1 \\ & P_q(\mathbf{u}_{\min} \leq \mathbf{u}_{t-1} \leq \mathbf{u}_{\max}) = 1 \\ & P_q(\mathbf{x}_{\min} \leq \mathbf{x}_t \leq \mathbf{x}_{\max}) = 1. \end{aligned} \quad (9)$$

Our goal is to solve the above optimization problem. However, for any practical algorithm, we cannot guarantee exact constraint satisfaction, both due to the potential non-convexity of the constraint functions and due to numerical issues. This is particularly true when planning online with limited computational time. Therefore we will evaluate our method according to both the cost of the resulting trajectories and the amount of constraint violation when optimizing within a fixed number of iterations.

VI. STEIN VARIATIONAL GRADIENT DESCENT

We develop an algorithm to solve the constrained variational inference objective in (9) based on Stein Variational Gradient Descent (SVGD) [36]. In this section we will give an overview of SVGD which forms the foundation of our method. SVGD is a variational inference technique that uses a non-parametric representation of the variational posterior. In our algorithm, we use SVGD to approximate the distribution $p(\tau|o=1)$ with particles, where each particle is a trajectory. Consider the variational inference problem

$$q^*(\mathbf{x}) = \arg \min_{q(\mathbf{x})} \mathcal{KL}(q(\mathbf{x})||p(\mathbf{x})) \quad (10)$$

where $\mathbf{x} \in \mathbb{R}^d$ and p and q are two probability density functions supported on \mathbb{R}^d . SVGD is based on the *Kernelized Stein Discrepancy* (KSD) [52], which is a measure of the discrepancy between two distributions p and q . The KSD is computed as the result of the following constrained functional maximization

$$\mathbb{S}(p, q) = \max_{\phi \in \mathcal{H}^d} \{\mathbb{E}_{\mathbf{x} \sim q}[\mathcal{A}_p \phi(\mathbf{x})] \text{ s.t. } \|\phi\|_{\mathcal{H}^d} \leq 1\} \quad (11)$$

where $\phi : \mathbb{R}^d \rightarrow \mathbb{R}^d$ is a function in a vector-valued Reproducing Kernel Hilbert Space (RKHS) \mathcal{H}^d with kernel \mathcal{K} . \mathcal{A}_p is the Stein operator

$$\mathcal{A}_p \phi(\mathbf{x}) = \nabla_{\mathbf{x}} \log p(\mathbf{x})^T \phi(\mathbf{x}) + \nabla_{\mathbf{x}} \cdot \phi(\mathbf{x}) \quad (12)$$

where $\nabla_{\mathbf{x}} \cdot \phi(\mathbf{x}) = \sum_{k=1}^d \partial_{x_k} \phi_k(\mathbf{x})$. It was established in [52] that $\mathbb{S}(q, p) = 0 \iff p = q$ for a strictly positive-definite kernel \mathcal{K} . To minimize the KL divergence SVGD considers the incremental transform $\mathbf{x}_\epsilon = \mathbf{x} + \epsilon \phi(\mathbf{x})$ where $\mathbf{x} \sim q(\mathbf{x})$ and ϵ is a scalar step-size parameter. The resulting distribution after applying the transform is $q_{[\epsilon\phi]}$. SVGD uses the following result

$$\nabla_{\epsilon} \mathcal{KL}(q_{[\epsilon\phi]}||p(\mathbf{x}))|_{\epsilon=0} = -\mathbb{E}_{\mathbf{x} \sim q}[\mathcal{A}_p \phi(\mathbf{x})] \quad (13)$$

which relates the Stein operator and the derivative of the KL divergence w.r.t the perturbation ϵ . We would like to select ϕ that maximally decreases the KL divergence. By considering $\phi \in \{\phi \in \mathcal{H}^d; \|\phi\|_{\mathcal{H}^d} \leq 1\}$ the optimal ϕ is the solution to the following constrained functional maximization

$$\phi^* = \arg \max_{\phi \in \mathcal{H}^d} \{-\nabla_{\epsilon} \mathcal{KL}(q_{[\epsilon\phi]}||p(\mathbf{x}))|_{\epsilon=0}, \text{ s.t. } \|\phi\|_{\mathcal{H}^d} \leq 1\}. \quad (14)$$

This maximization has a closed-form solution, derived by Liu et al. in Theorem 3.8 of [52]. Note that we have used a slightly different definition of the Stein operator than that used by Liu et al., with \mathcal{A}_p as defined in equation (12) as equal to the trace

of the Stein operator defined in [52]. The closed-form solution is given by

$$\phi^*(\cdot) = \mathbb{E}_{\mathbf{x} \sim q}[\mathcal{A}_p \mathcal{K}(\cdot, \mathbf{x})] \quad (15)$$

and the resulting gradient of the KL divergence is

$$\nabla_{\epsilon} \mathcal{KL}(q_{[\epsilon^* \phi]} \| p(\mathbf{x}))|_{\epsilon=0} = -\mathbb{S}(p, q). \quad (16)$$

This implies that for a suitably-chosen kernel \mathcal{K} , if the gradient of the KL divergence is zero then the KSD is also zero, which means that $p = q$. SVGD uses these ideas to propose an iterative algorithm for approximating distribution p with a particle representation of $q(\mathbf{x}) = \frac{1}{N} \sum_{i=1}^N \delta(\mathbf{x} - \mathbf{x}^i)$. SVGD updates the particle set with

$$\mathbf{x}_{k+1}^i = \mathbf{x}_k^i + \epsilon \phi^*(\mathbf{x}_k^i). \quad (17)$$

The closed-form solution in equation (15) is approximated with a set of particles as

$$\phi^*(\mathbf{x}_k^i) = \frac{1}{N} \sum_{j=1}^N \mathcal{K}(\mathbf{x}_k^i, \mathbf{x}_k^j) \nabla_{\mathbf{x}_k^j} \log p(\mathbf{x}_k^j) + \nabla_{\mathbf{x}_k^j} \mathcal{K}(\mathbf{x}_k^i, \mathbf{x}_k^j). \quad (18)$$

The first term of this objective maximizes the log probability $p(\mathbf{x})$ for the particles. The second term is a repulsive term that acts to push particles away from one another and prevents the particle set from collapsing to a local MAP solution.

A. Orthogonal-Space Stein Variational Gradient Descent

Recently Zhang et. al. proposed O-SVGD, a method for performing SVGD with a single equality constraint [11], though they do not consider the problem of trajectory optimization. In this section, we give an overview of O-SVGD, but we give an alternative derivation to that given in [11] based on vector-valued RKHS and matrix-valued kernels [53]. This alternative derivation will allow us to analyze our algorithm (Section VII-A3). The problem [11] aims to solve is

$$\min_q \mathcal{KL}(q(\mathbf{x}) \| p(\mathbf{x})) \quad \text{s.t.} \quad P_q(h(\mathbf{x}) = 0) = 1 \quad (19)$$

where h represents a single equality constraint. For particles \mathbf{x} that are on the manifold induced by $h(\mathbf{x}) = 0$, we would like them to remain on the manifold after applying the Stein update in equation (17). To do this, we replace the function $\phi(\mathbf{x})$ with $P(\mathbf{x})\phi(\mathbf{x})$. Where $P(\mathbf{x})$ projects the updates to be in the tangent-space of the constraint and is given by

$$P(\mathbf{x}) = I - \frac{\nabla h(\mathbf{x}) \nabla h(\mathbf{x})^T}{\|\nabla h(\mathbf{x})\|^2}. \quad (20)$$

We can develop an SVGD algorithm that updates particles on the constraint manifold by considering the set of functions $\{P(\mathbf{x})\phi(\mathbf{x}), \phi(\mathbf{x}) \in \mathcal{H}^d\}$. By applying Lemma 2 from [53] we establish that this set of functions is a RKHS \mathcal{H}_{\perp}^d with matrix-valued kernel \mathcal{K}_{\perp} given by

$$\mathcal{K}_{\perp}(\mathbf{x}^i, \mathbf{x}^j) = \mathcal{K}(\mathbf{x}^i, \mathbf{x}^j) P(\mathbf{x}^i) P(\mathbf{x}^j). \quad (21)$$

Running SVGD with kernel \mathcal{K}_{\perp} will therefore solve the constrained minimization problem (14), maximally reducing the KL divergence while only considering updates that lie in the tangent-space of the constraint. Zhang et. al. [11] also add

a term to equation (17) that drives particles to the manifold induced by the constraint

$$\phi_C = -\frac{\psi(h(\mathbf{x})) \nabla h(\mathbf{x})}{\|\nabla h(\mathbf{x})\|^2} \quad (22)$$

where ψ is an increasing odd function.

VII. METHODS

Our proposed trajectory optimization algorithm uses SVGD to perform a constrained optimization on a set of trajectories in parallel. The result is a diverse set of low-cost constraint-satisfying trajectories. The full algorithm is shown in Algorithm 1. First, we will introduce the main component of our proposed algorithm, which decomposes the Stein update into a step tangential to the constraint boundary, and a step toward constraint satisfaction. We will then provide an analysis of the algorithm which relates it to problem (9). Finally, we will discuss strategies for improving performance which include separating the bounds constraints, an annealing strategy for increasing particle diversity, and re-sampling particles during the optimization. Figure 2 demonstrates CSVTO being applied to a 2D toy problem.

A. Constrained Stein Trajectory Optimization

Solving the constrained variational inference problem in (9) is very difficult, since it requires finding a distribution that may exhibit multi-modality and has constrained support. To deal with this, we adopt a non-parametric approach to representing distribution $q(\tau)$. We use SVGD where each particle is a trajectory, and iteratively update the particle set while enforcing the constraints on each particle. To do this we extend O-SVGD to arbitrary equality and inequality constraints and use it to generate constraint-satisfying trajectories.

First, we relate using SVGD for unconstrained trajectory optimization to the minimization of the unconstrained variational free energy $\mathcal{F}(q)$ from (6). Consider the iterative transform $\tau_{\epsilon} = \tau + \epsilon \phi^*(\tau)$, where ϕ^* is the solution to (14) with posterior log likelihood $\log p(\tau | o = 1)$, $\tau \sim q(\tau)$ and $\tau_{\epsilon} \sim q_{[\epsilon \phi^*]}(\tau)$. We can recast (14) for trajectories in terms of the free energy $\mathcal{F}(q)$

$$\phi^*(\tau) = \arg \max_{\phi \in \mathcal{H}^d} \{-\nabla_{\epsilon} \mathcal{F}(q_{[\epsilon \phi]})|_{\epsilon=0}, \text{s.t.} \|\phi\|_{\mathcal{H}^d} \leq 1\}. \quad (23)$$

Thus the update $\tau + \epsilon \phi^*$ ensures we maximally decrease the variational free energy. If $\phi^*(\tau) = 0$ then $q(\tau)$ is at a local minima of $\mathcal{F}(q)$. We will now modify the Stein update to account for constraints.

1) *Equality constraints:* We propose a modified Stein update rule in which we decompose the update into two components:

$$\tau_{k+1}^i = \tau_k^i + \alpha_J \phi_{\perp}(\tau_k) + \alpha_C \phi_C(\tau_k^i) \quad (24)$$

where ϕ_{\perp} is an update that is tangential to the constraint boundary, ϕ_C acts in the direction which decreases constraint violation, and α_J and α_C are scalar step size parameters. We replace the O-SVGD ϕ_C from equation (22) with a Gauss-Newton step to minimize $h(\tau)^T h(\tau)$.

$$\phi_C = \nabla h^T (\nabla h \nabla h^T)^{-1} h. \quad (25)$$

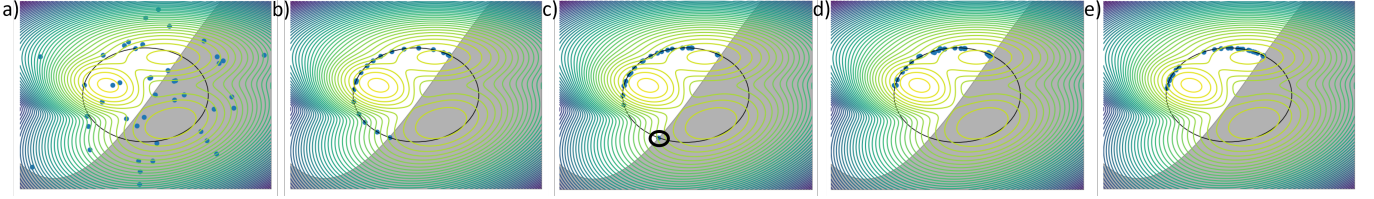


Fig. 2. CSVTO visualized for a 2D problem. The posterior is a mixture of 3 Gaussians, with the log posterior peaks visualized. There is an equality constraint that the particles must lie on the circle. There is also an inequality constraint that the particles must lie outside the shaded region. a) The initial particles are randomly generated and are not necessarily feasible. b) Due to the annealing discussed in section VII-A4, early on in the optimization the particles are constraint satisfying and diverse. c) The particles move towards the relative peaks of the objective, however, the circled particle has become stuck in a poor local minimum due to the constraints. d) The resampling step from section VII-A8 resamples the particles, applying noise in the tangent-space of the constraints. This eliminates the particle at the poor local minima. e) The set of particles converges around the local minima of the objectives while satisfying the constraints.

This uses approximate second-order curvature information for fast convergence. We then compute the *projection* matrix $P(\tau)$, which projects vectors onto the tangent space of the constraints as

$$P(\tau) = I - \nabla h(\tau)^T (\nabla h(\tau) \nabla h(\tau)^T)^{-1} \nabla h(\tau). \quad (26)$$

Performing this inverse is only possible if $\nabla h(\tau)$ is full rank. If it is not full rank, we instead use the pseudo-inverse of $\nabla h(\tau) \nabla h(\tau)^T$. Once we have $P(\tau)$, we can use it to define the tangent-space kernel, as in [11]:

$$\mathcal{K}_\perp(\tau^i, \tau^j) = \mathcal{K}(\tau^i, \tau^j) P(\tau^i) P(\tau^j). \quad (27)$$

We can then use this kernel for the SVGD update to produce an update that is in the tangent space of the constraint:

$$\begin{aligned} \phi_\perp^*(\tau^i) &= \frac{1}{N} \sum_{j=1}^N \mathcal{K}_\perp(\tau^i, \tau^j) \nabla_{\tau^j} \log p(\tau^j | o=1)(\tau^j) \\ &\quad + \nabla_{\tau^j} \mathcal{K}_\perp(\tau^i, \tau^j). \end{aligned} \quad (28)$$

Since \mathcal{K}_\perp is a matrix-valued function, the last term is calculated as

$$[\nabla_{\tau^j} \mathcal{K}_\perp(\tau^i, \tau^j)]_l = \sum_m \nabla_{[\tau^j]_m} [\mathcal{K}_\perp(\tau^i, \tau^j)]_{lm} \quad (29)$$

where the notation $[x]_l$ indicates the l th index of x . Equation (28) has several interesting features. First, two trajectory particles τ^i and τ^j are considered close if they are close according to the original kernel \mathcal{K} . In addition, expanding the first term to $\mathcal{K}(\tau^i, \tau^j) P(\tau^i) P(\tau^j) \nabla_{\tau^j} \log p(\tau^j | o=1)$, we see that if $P(\tau^i) = P(\tau^j)$ this reduces to $\mathcal{K}(\tau^i, \tau^j) P(\tau^j) \nabla_{\tau^j} \log p(\tau^j | o=1)$. For $P(\tau^i) \neq P(\tau^j)$, the magnitude of this term will always be reduced. Intuitively this means that particles will share gradients if particles are close and the tangent space of the constraint is similar. In addition, all updates will be in the tangent space of the constraint. The term $\nabla_{\tau^j} \mathcal{K}_\perp(\tau^i, \tau^j)$ will repulse the particles away from one another in the tangent-space of the constraint. Note that computing the term $\nabla_{\tau^j} \mathcal{K}_\perp(\tau^i, \tau^j)$ requires the evaluation of the second derivative of the constraint function $\nabla^2 h(\tau)$. We will discuss how we define a kernel on trajectories in section VII-A5.

2) *Extension to Inequality Constraints:* We extend the above method to inequality constraints with the use of slack variables. We turn the inequality constraints into equality constraints with slack variable z :

$$g(\tau) + \frac{1}{2} z^2 = 0. \quad (30)$$

We then compute the constrained Stein update with all constraints as equality constraints. The full set of equality constraints then becomes

$$\hat{h} = \begin{bmatrix} h(\tau) \\ g(\tau) + \frac{1}{2} z^2 \end{bmatrix}. \quad (31)$$

We augment the state with z as

$$\hat{\tau} = \begin{bmatrix} \tau \\ z \end{bmatrix}. \quad (32)$$

The projection is given by

$$P(\hat{\tau}) = I - \nabla \hat{h}^T (\nabla \hat{h} \nabla \hat{h}^T)^{-1} \nabla \hat{h} \quad (33)$$

and the kernel is

$$\mathcal{K}_\perp(\hat{\tau}^i, \hat{\tau}^j) = \mathcal{K}(\tau^i, \tau^j) P(\hat{\tau}^i) P(\hat{\tau}^j). \quad (34)$$

Notice that the kernel uses the original τ and not the augmented $\hat{\tau}$. We then perform the constrained Stein update on the augmented state:

$$\begin{aligned} \phi_\perp^*(\hat{\tau}^i) &= \frac{1}{N} \sum_{j=1}^N \mathcal{K}_\perp(\hat{\tau}^i, \hat{\tau}^j) \begin{bmatrix} \nabla \log p(\tau^j | o=1) \\ 0 \end{bmatrix} \\ &\quad + \nabla_{\hat{\tau}^j} \mathcal{K}_\perp(\hat{\tau}^i, \hat{\tau}^j) \end{aligned} \quad (35)$$

$$\phi_C = \nabla \hat{h}^T (\nabla \hat{h} \nabla \hat{h}^T)^{-1} \hat{h}. \quad (36)$$

Once we have performed the iterative optimization we have a set of trajectories. We then select a trajectory to execute by choosing the one which minimizes the penalty function

$$\hat{C}_\lambda(\tau) = C(\tau) + \lambda \sum |\hat{h}|. \quad (37)$$

3) *Analysis:* In this section, we provide an analysis of CSVTO. We demonstrate that stationary points of the gradient flow satisfy the first-order optimality conditions for the constrained variational optimization problem in (9), subject only to equality constraints. Fukuda and Fukushima established the conditions for the equivalence of the first-order optimality conditions for problems with both inequality and

equality constraints, and the corresponding equality-constrained reformulation with slack variables [54].

Theorem 1. *Assume that ∇h is full rank. Let $\phi^* \in \mathcal{H}^d$ be the solution to (14) with the unconstrained kernel \mathcal{K} , and $\phi_\perp^* \in \mathcal{H}_\perp^d$ be the solution to (14) using the tangent-space kernel \mathcal{K}_\perp . If the following holds*

$$\alpha_J \phi_\perp^*(\tau) + \alpha_C \phi_C(\tau) = 0, \quad (38)$$

then the following must be true:

$$\phi^*(\tau) + \nabla h(\tau)^T \mu = 0 \quad (39)$$

$$h(\tau) = 0 \quad (40)$$

where μ is a vector of Lagrange multipliers.

Proof. Since ϕ_C and ϕ_\perp^* are orthogonal, then if equation (38) holds then $\phi_C = \phi_\perp^* = 0$. Next, we note that $\phi_\perp^*(\tau) = P(\tau)\hat{\phi}$, where $\hat{\phi} \in \mathcal{H}^d$ and further $P(\tau)\hat{\phi}(\tau) = 0 \implies P(\tau)\phi^*(\tau) = 0$. To see this, consider $P(\tau)\phi^*(\tau) \neq 0$. This would imply that $\nabla_\epsilon \mathcal{K}\mathcal{L}(q_{[\epsilon P\phi^*]} || p(\tau|o = 1))|_{\epsilon=0} \neq 0$, which implies that there is a descent direction. This would mean that $\exists \phi_\perp$ such that $-\nabla_\epsilon \mathcal{K}\mathcal{L}(q_{[\epsilon \phi_\perp]} || p(\tau|o = 1))|_{\epsilon=0} < -\nabla_\epsilon \mathcal{K}\mathcal{L}(q_{[\epsilon \phi_\perp]} || p(\tau|o = 1))|_{\epsilon=0}$, which is a contradiction. Expanding $P(\tau)\phi^* = 0$ yields

$$\begin{aligned} [I - \nabla h(\tau)^T (\nabla h(\tau) \nabla h(\tau)^T)^{-1} \nabla h(\tau)] \phi^*(\tau) &= 0 \\ \phi^*(\tau) - \nabla h(\tau)^T [(\nabla h(\tau) \nabla h(\tau)^T)^{-1} \nabla h(\tau) \phi^*(\tau)] &= 0 \end{aligned} \quad (41)$$

Specifying $\mu = -(\nabla h(\tau) \nabla h(\tau)^T)^{-1} \nabla h(\tau) \phi^*(\tau)$ results in equation (39) being satisfied. Now we expand $\phi_C = 0$ resulting in

$$\nabla h(\tau)^T (\nabla h(\tau) \nabla h(\tau)^T)^{-1} h(\tau) = 0. \quad (42)$$

To show feasibility at the stationary point we left multiply (42) by $\nabla h(\tau)$, which for full rank ∇h results in $h(\tau) = 0$. \square

Theorem 1 holds when we can integrate the expectation in (15). However, we are approximating the expectation with particles so (39) may not hold in practice. However, the feasibility condition (40) remains true when using a particle approximation for q .

4) *Annealed SVGD for improved diversity:* We employ an annealing technique for SVGD as proposed in [55]. We use a parameter $\gamma \in [0, 1]$ which controls the trade-off between the gradient of the posterior log-likelihood and the repulsive gradient. For $\gamma \ll 1$ the repulsive term dominates resulting in trajectories being strongly forced away from one another. As γ increases the gradient of the posterior likelihood has a greater effect resulting in trajectories being optimized to decrease the cost. When combined with ϕ_C this results in the optimization prioritizing diverse constraint-satisfying trajectories first, then decreasing cost later in the optimization. The annealed update is given by

$$\begin{aligned} \phi_\perp^i(\hat{\tau}) &= \frac{1}{N} \sum_{j=1}^N \gamma \mathcal{K}_\perp(\hat{\tau}_i, \hat{\tau}_j) \begin{bmatrix} \nabla \log p(\tau_j|o) \\ 0 \end{bmatrix} \\ &+ \nabla_{\hat{\tau}_j} \mathcal{K}_\perp(\hat{\tau}_i, \hat{\tau}_j). \end{aligned} \quad (43)$$

We use a linear annealing schedule with $\gamma_k = \frac{k}{K}$, where K is the total number of iterations. When performing online re-planning, we only perform the annealing when optimizing the trajectory the first time-step.

5) *Trajectory Kernel:* CSVTO relies on a base kernel $\mathcal{K}(\tau^i, \tau^j)$ operating on pairs of trajectories which defines the similarity between trajectories. As noted by Lambert et. al. [10], high dimensional spaces can result in diminishing repulsive forces. This can be problematic for trajectory optimization problems due to the time horizon. We use a similar approach to SVMPC [10] in that we decompose the kernel into the sum of kernels operating on smaller components of the trajectory. We use a sliding window approach to decompose the trajectory. For a given sliding window length W let $\tau^t = [x_{t:t+W}, u_{t-1:t-1+W}]^T$. The overall kernel is then given by

$$\mathcal{K}(\tau^i, \tau^j) = \frac{1}{T-W} \sum_t^{T-W} \mathcal{K}(\tau_t^i, \tau_t^j). \quad (44)$$

We use the RBF kernel $\mathcal{K}(\tau_t^i, \tau_t^j) = \exp(-\frac{1}{h} \|\tau_t^i - \tau_t^j\|^2)$ as the base kernel, where h is the kernel bandwidth. We use the median heuristic as in [36] to select the kernel bandwidth:

$$h = \frac{\text{median}(\|\tau_t^i - \tau_t^j\|)^2}{\log(N)} \quad (45)$$

where N is the number of particles.

6) *Bounds constraint:* Bounds constraints can, in principle, be handled as general inequality constraints as described in the above section. However, since this involves adding additional slack variables incorporating bounds constraints involves an additional $T \times 2(d_u + d_x)$ decision variables in the optimization, where d_x and d_u are the state and control dimensionalities respectively. It is more computationally convenient to use a simple approach where at every iteration we directly project the trajectory to satisfy the bound constraints. This is done by

$$u^* = \min(\max(u_{min}, u), u_{max}). \quad (46)$$

7) *Shift operation:* When running trajectory optimization online in an MPC style-loop as in Algorithm 2, it is typical to warm-start the optimization with the solution from the previous timestep. For a single particle, the trajectory consists of $\tau = (x_1, \dots, x_T, u_0, \dots, u_{T-1})$. The shift operation computes $\tau' = (x_2, \dots, x'_{T+1}, u_1, \dots, u'_T)$. Here x'_{T+1}, u'_T is the initialization for the newly considered future timestep. The initializations x'_{T+1}, u'_T may be chosen in a problem-specific way. In our approach, we choose them by sampling the control from the prior $p(u)$ and computing the corresponding next state. The above heuristic is motivated by the assumption that the solution should not vary much between timesteps. However, the fact that we have a set of trajectories rather than a single one can invalidate this assumption, since we can only take a single action. This means that trajectories that have very different first actions from the action we took can end up being quite poor initializations, particularly in the presence of constraints that can render them infeasible. This motivates the next section in which we discuss a resampling technique to prevent sample impoverishment.

8) *Resampling*: As discussed above, the shift operation can lead to trajectories that are not executed becoming infeasible and rendering those particles useless for trajectory optimization. In addition, our cost and constraints are not necessarily convex, so, as with any local optimization method, poor initializations can lead to infeasibility. We take inspiration from the Particle Filter literature [56] and incorporate a resampling step which is executed when performing online re-planning. Every `resample_steps` timesteps we resample after performing the shift operation on the previous trajectory particles. To perform resampling, we compute weights using the penalty function

$$w_i = \frac{\exp(-\frac{\hat{C}_\lambda(\tau_i)}{\beta})}{\sum_j^N \exp(-\frac{\hat{C}_\lambda(\tau_j)}{\beta})} \quad (47)$$

where β is a temperature parameter. We then resample a new set of particles according to weights w_i . It is common in the particle filter literature to additionally add noise, to prevent resampled particles collapsing. However, in our case, it is undesirable to add random noise to a constraint-satisfying trajectory as it may lead to constraint violation. We avoid this issue by sampling noise and projecting the noise to only have components in the tangent space of the constraints for a given trajectory. Suppose we have sampled trajectory τ_i from the set of particles. We first sample $\epsilon \sim \mathcal{N}(0, \sigma_{resample}^2 I)$, and then update the trajectory with

$$\tau_{new} = \tau_i + P(\tau_i)\epsilon \quad (48)$$

where $P(\tau_i)$ is the projection matrix from equation (26).

Algorithm 1 A single step of CSVTO, this will run every timestep.

Inputs:

```

1: function CSVTO( $x_0, \tau, K, \text{anneal}$ )
2:   for  $k \in \{1, \dots, K\}$  do
3:     for  $i \in \{1, \dots, N\}$  do
4:        $\phi_C^i \leftarrow$  via eq. 36
5:       if anneal then
6:          $\gamma \leftarrow \frac{k}{K}$ 
7:          $\phi_\perp^i \leftarrow$  via eq. 43
8:       else
9:          $\phi_\perp^i \leftarrow$  via eq. 35
10:       $\tau^i \leftarrow \tau^i + \alpha_J \phi_\perp^i + \alpha_C \phi_C^i$ 
11:       $\tau^i \leftarrow$  PROJECTINBOUNDS( $\tau^i$ ).
12:   return  $\tau$ 

```

VIII. EVALUATION

We evaluate our approach in three experiments. The first is a constrained 12DoF quadrotor task which has nonlinear underactuated dynamics. The second experiment is a 7DoF robot manipulator task, where the aim is to move the robot end-effector to a goal location while being constrained to move along the surface of a table. The third experiment is also a 7DoF robot manipulator task, where the aim is to manipulate a wrench to a goal angle. Both of these 7DoF manipulator

Algorithm 2 CSVTO running with online re-planning

```

1: function CSVTO_MPC( $x_0, \tau_0$ )
2:   for  $t \in \{1, \dots, T\}$  do
3:      $\triangleright$  Resample
4:     if MOD( $t, \text{resample\_steps}$ ) = 0 then
5:        $\tau_t \leftarrow$  RESAMPLE( $\tau_t$ )
6:     if  $t = 1$  then
7:        $K \leftarrow K_{warmup}$ 
8:       anneal  $\leftarrow$  True
9:     else
10:       $K \leftarrow K_{online}$ 
11:      anneal  $\leftarrow$  False
12:       $\tau_t \leftarrow$  CSVTO( $x_t, \tau_t, K, \text{anneal}$ )
13:       $\triangleright$  Select trajectory according to penalty function
14:       $\tau^* \leftarrow \arg \min_\tau \hat{C}_\lambda(\tau)$ 
15:       $\triangleright$  Select first control
16:       $u_t \leftarrow \tau^*$ 
17:       $x_t \leftarrow$  STEPENV( $u_t$ )
18:       $\triangleright$  Shift operation
19:       $\tau_{t+1} \leftarrow$  SHIFT( $\tau_t$ )

```

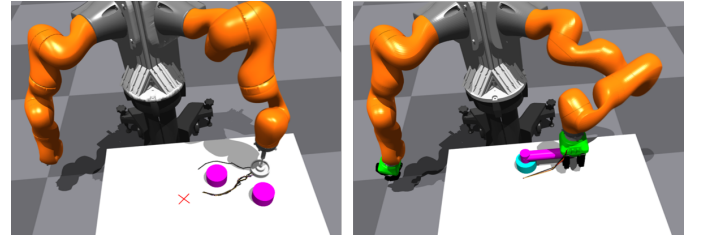


Fig. 3. Left) Experimental set-up for the robot manipulator on a surface experiment. The robot must move the end effector to the goal, shown in red while keeping the end effector on the surface and avoiding the purple obstacles. CVTO plans multi-modal trajectories which avoid the obstacle and satisfy constraints. Right) The robot manipulator turning a wrench experimental set-up. The goal is to turn the wrench by 90 degrees.

tasks involve planning in highly constrained domains. We perform the manipulator experiments in IsaacGym [57]. The hyperparameters we use in all experiments are shown in Table I. For all experiments, the costs and constraint functions are written using PyTorch [58], and automatic differentiation is used to evaluate all relevant first and second derivatives.

A. Baselines

We compare our trajectory optimization approach to both sampling-based and gradient-based methods. We compare against IPOPT [12], a general non-linear constrained optimization solver, which has been widely used for robot trajectory optimization [4], [13]. We use the MUMPS [59] linear solver, and supply IPOPT with the exact Hessians evaluated using automatic differentiation. We additionally compare against MPPI [30] and SVMPC [10]. MPPI and SVMPC are methods for performing unconstrained trajectory optimization, with constraints commonly incorporated with penalties. We test both of these methods with penalties of $\lambda = 100$ and $\lambda = 1000$. In the SVMPC paper, the authors show that their method can be used both with and without gradients. We evaluate against two

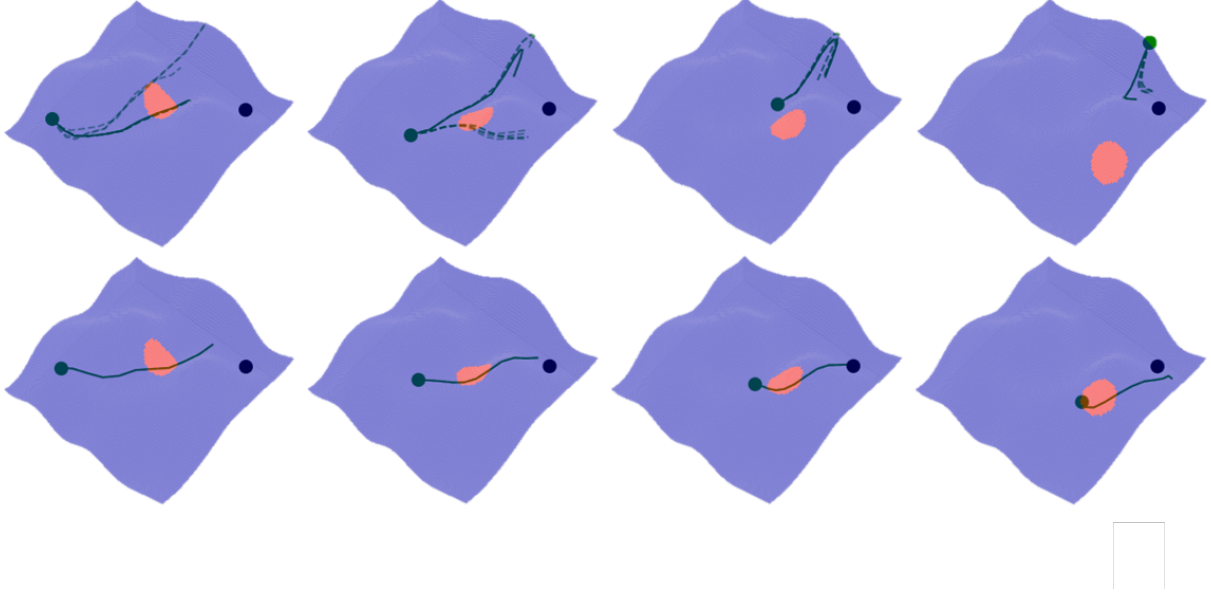


Fig. 4. Experimental setup for the quadrotor task. The quadrotor must travel to the goal location, avoiding the obstacle in red while remaining on the blue manifold. Top) CSVTO maintains a set of trajectories, with the selected trajectory shown in solid. CSVTO can keep a diverse set of trajectories and switches between them to avoid the moving obstacle. Bottom) IPOPT generates an initial trajectory that makes good progress toward the goal while avoiding the obstacle and obeying the manifold constraint. However, as the obstacle moves IPOPT is unable to find an alternative trajectory and ends in a collision.

versions of SVMPC, one using a sample-based approximation to the gradient and another using the true gradient. Note that for our approach and IPOPT, we use a direct transcription scheme; IPOPT solves the optimization problem as expressed in problem (1). In contrast, for SVMPC and MPPI we use a shooting scheme since they can only handle constraints via penalties, which can lead to poor satisfaction of the dynamics constraint.

B. 12DoF Quadrotor

We evaluate our method on a 12DoF underactuated quadrotor problem. The goal is to navigate the quadrotor from a start state to a goal state. We chose this problem to demonstrate our approach on a problem with complex nonlinear underactuated dynamics. The experimental setup is shown in Figure 4. The state of the quadrotor is 6DoF pose parameterized with Euler angles and linear and angular velocities. The dynamics for the 12DoF quadrotor are from [60] and are given by

$$\begin{bmatrix} x \\ y \\ z \\ p \\ q \\ r \\ \dot{x} \\ \dot{y} \\ \dot{z} \\ \dot{p} \\ \dot{q} \\ \dot{r} \end{bmatrix}_{t+1} = \begin{bmatrix} x \\ y \\ z \\ p \\ q \\ r \\ \dot{x} \\ \dot{y} \\ \dot{z} \\ \dot{p} \\ \dot{q} \\ \dot{r} \end{bmatrix}_t + \Delta t \begin{bmatrix} \dot{x} \\ \dot{y} \\ \dot{z} \\ \dot{p} + \dot{q}s(p)t(q) + \dot{r}c(p)t(q) \\ \dot{q}c(p) - \dot{r}s(p) \\ \dot{q}\frac{s(p)}{c(q)} + \dot{r}\frac{c(p)}{c(q)} \\ -(s(p)s(r) + c(r)c(p)s(q))K\frac{u_1}{m} \\ -(c(r)s(p) - c(p)s(r)s(q))K\frac{u_1}{m} \\ g - c(p)s(q)K\frac{u_1}{m} \\ \frac{(I_y - I_z)\dot{q}\dot{r} + Ku_2}{I_x} \\ \frac{(I_z - I_x)\dot{p}\dot{r} + Ku_3}{I_y} \\ \frac{(I_x - I_y)\dot{p}\dot{q} + Ku_4}{I_z} \end{bmatrix}_t \quad (49)$$

where $c(p), s(p), t(p)$ are cos, sin, tan functions respectively. We use parameters $m = 1, I_x = 0.5, I_y = 0.1, I_z = 0.3, K = 5, g = -9.81$. The constraints for this system are that the quadrotor must travel along a nonlinear surface $z = f(x, y)$. For this surface, we sample a function from a Gaussian prior with an RBF kernel and zero mean function. In addition, we include a cylindrical obstacle in the x-y plane that the quadrotor must avoid. This obstacle moves during the trial in a path that is unknown to the planner; at every timestep, the planner plans assuming the obstacle will remain fixed. The posterior $\log p(\tau|o)$ for this problem is a quadratic cost $(x - x_{goal})^T P(x - x_{goal}) + \sum_{t=1}^T (x - x_{goal})^T Q(x_t - x_{goal}) + u_{t-1}^T R u_{t-1}$. The control cost is equivalent to the prior on controls $p(u_t) = \mathcal{N}(0, R^{-1})$.

We run this experiment for 20 trials with randomly sampled starts. We additionally run this experiment under three conditions: 1) no obstacle; 2) a static obstacle; and 3) a dynamic obstacle. The results are shown in Figure 5. CSVTO can succeed for 20/20 trials in all cases with a goal threshold of 0.8m and has achieves an 80% success rate for a goal region of 0.5m. For the static-obstacle and no-obstacle experiments, IPOPT is the next best performing with 20/20 trials at a goal threshold of 0.8m but fails when the obstacle is dynamic, achieving only a 15% success rate. Trajectories generated from IPOPT vs CSVTO are shown in Figure 4, IPOPT generates a good initial trajectory, but the movement of the obstacle renders that trajectory infeasible as time progresses. IPOPT is not able to adapt the trajectory to go around the obstacle. In contrast, CSVTO generates a multimodal set of trajectories that go either way around the obstacle. It is then able to update the trajectories effectively and avoid the obstacle, reaching the goal. We do see that IPOPT achieves the lowest constraint violation in the case of no obstacle or a static obstacle, while

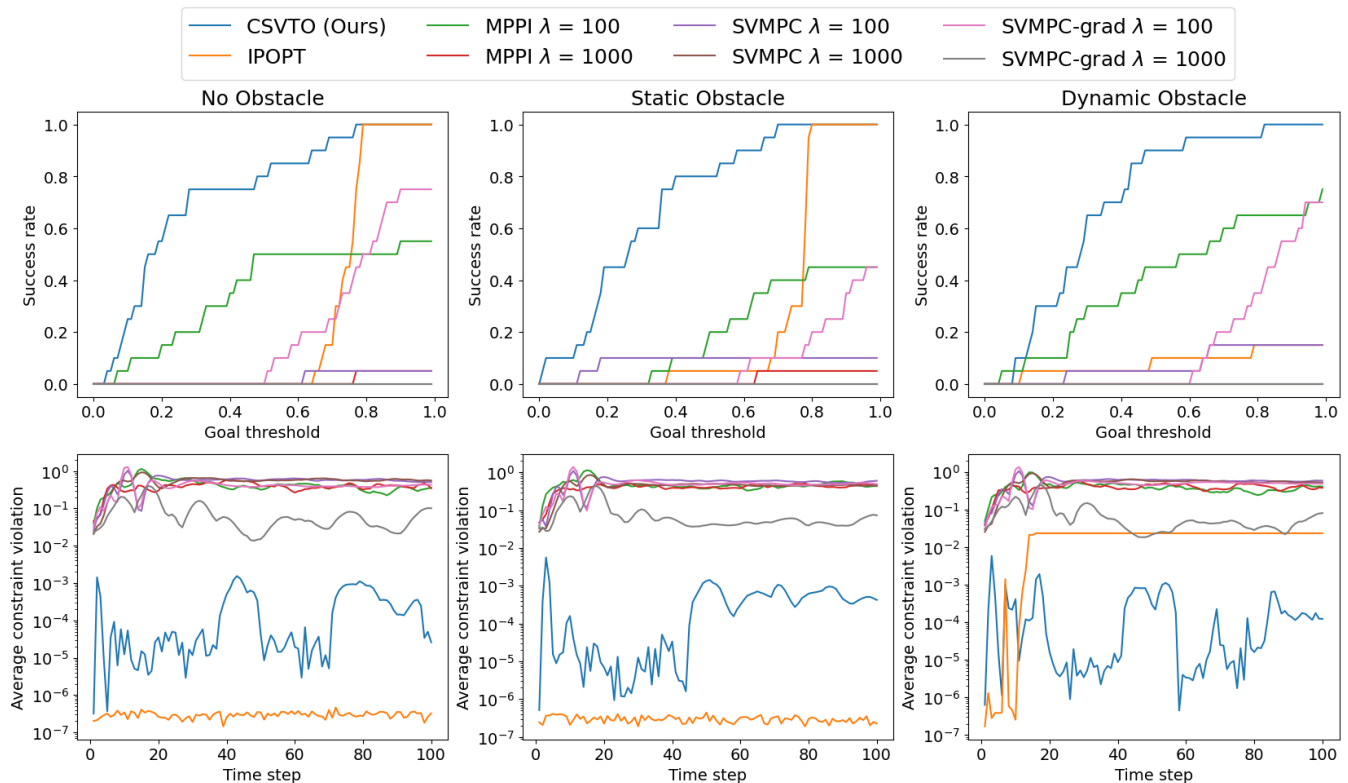


Fig. 5. Results for quadrotor experiments. The top row shows the success rate as we increase the size of the goal region. The bottom row shows the average constraint violation as a function of time. (Left) No obstacle. (Middle) Static obstacle. (Right) Dynamic obstacle.

CSVTO achieves the lowest constraint violation when there is a dynamic obstacle. SVMPC-grad performs well according to success rate for all experiments but has very poor constraint violation. We see that sample-based methods fail to complete the task and satisfy the constraints.

C. Robot Manipulator on Surface

In this task, we consider a 7DoF robot manipulator where the end effector is constrained to move along a surface to a goal location while avoiding obstacles on the surface. The set-up is shown in Figure 3. This system’s state space is the robot’s joint configuration $q \in \mathbb{R}^d$. The actions are the joint velocity \dot{q} and the dynamics are given by Euler integration $q_{t+1} = q_t + \dot{q}_t dt$, with $dt = 0.1$. The prior distribution over actions is $p(U) = \mathcal{N}(0, \sigma^2 I)$, where $\sigma^2 = [0.1, 0.125, 0.15, 0.2, 0.3, 0.5, 1.0]^T$. This results in a prior cost on path length that is scaled such that joints closer to the base of the robot are penalized more. The cost is $C(\tau) = 20\|p_T^{xy} - p_{goal}^{xy}\|_2 + \sum_{t=1}^{T-1} \|p_t^{xy} - p_{goal}^{xy}\|_2$, where p_t^{xy} is the end effector x, y position which is computed from the forward kinematics. The equality constraints on this system are $p_t^z = 0.8$ which is the height of the table, and additionally, there is an orientation constraint that the z -axis of the robot end effector must be orthogonal to the table. The inequality constraints are that the robot end effector must avoid two cylindrical obstacles on the surface of the table. There are also joint limits on all of the robot joints. We run this experiment for 20 trials with random goals and show the results in the top row of Figure 6. Our results show that

CSVTO succeeds in all 20 trials with a goal threshold of 0.05m. The next closest baseline, IPOPT succeeds 19/20 times. CSVTO achieves the lowest constraint violation early on in the trajectory, while IPOPT reduces the violation further along in the trajectory. All penalty-based methods have poor constraint violation.

D. Robot Manipulator using wrench

In this task we consider a 7DoF robot manipulator in which the goal is to manipulate a wrench to a goal angle. To turn the wrench, the robot must be able to supply at least 1Nm of torque. The set-up is shown in Figure 3. The state space is $[q \ \phi \ \theta]^T$. $q \in \mathbb{R}^7$ is the configuration space of the robot. ϕ parameterizes the distance between the robot end-effector and the wrench in the x - y plane as $l + \phi$ where l is a nominal distance. θ is the wrench angle. The actions are the joint velocities \dot{q} . The dynamics of the joint configuration are given by Euler integration $q_{t+1} = q_t + \dot{q}_t dt$, with $dt = 0.1$. We use a simple geometric model for dynamics of ϕ and θ . Assuming that the robot end-effector remains grasping the wrench we compute the next ϕ as $\phi = \|p_{ee}^{xy} - p_{wrench}^{xy}\|_2 - l$. To compute the next joint angle θ we use $\theta_{t+1} = \theta_t + \tan^{-1} \frac{\Delta x_{ee}}{\Delta y_{ee}}$. The prior distribution over actions is $p(U) = \mathcal{N}(0, \sigma^2 I)$, where $\sigma^2 = [0.1, 0.125, 0.15, 0.2, 0.3, 0.5, 1.0]^T$. The equality constraints of the system are that p_{ee}^z should be at a fixed height, and additionally that $\theta_T = \theta_{goal}$. The inequality constraints of the system are that the desired torque should be achievable within the robot joint limits. This constraint is $\min_torque \leq$

Experiment	# particles	α_J	α_C	ϵ	K_{warmup}	K_{online}	resample_steps	β	$\sigma_{resample}$	λ	W
Quadrotor	8	0.1	1	0.5	100	10	5	0.25	0.1	1	3
Manipulator on Surface	8	5×10^{-3}	1	0.25	100	10	1	0.1	0.01	1000	3
Manipulator wrench	4	0.01	1	0.1	100	10	1	0.1	0.01	1000	3

TABLE I

HYPERPARAMETER VALUES FOR THE THREE EXPERIMENTS

$J(q)^T(l + \phi) \leq \max_torque$ where J is the manipulator jacobian. There are also joint limit bound constraints, and a bound constraint on ϕ . There is no cost C for this experiment, instead, the inference problem reduces to conditioning the prior on constraint satisfaction. We run this experiment for 20 trials with random initializations and show the results in the bottom row of Figure 6. This problem is challenging because the dynamics are based on a simple inaccurate geometric model. Compliance in the gripper causes deviation from this geometric model, and the model is only accurate so long as all constraints hold. Our results show that CSVTO can succeed in all 20 trials with a goal threshold of 0.08 radians. The next closest baseline, IPOPT succeeds 13/20 times, while SVMPC-grad succeeds in 12/20 times. CSVTO achieves the lowest constraint violation for this problem. In this experiment we see that sample-based methods have poor constraint violation and poor performance.

We also demonstrate CSVTO on real hardware for the robot manipulator manipulating a wrench task, shown in Figure 1. We use the same hyperparameters as those in the simulator for this experiment. During execution, we applied disturbances by perturbing the robot end-effector. Figure 1 shows one such perturbation. Despite strong disturbances, our method was able to readjust the grasp and complete the task successfully.

E. Computation Time

The average computation time of CSVTO compared to baselines is shown in Table II. These are based on the average computation times recorded when running all experiments on a computer with an Intel i9-11900KF Processor with a NVIDIA RTX 3090 GPU. For IPOPT we use the open source implementation provided by [12], CSVTO and all other baselines are implemented in PyTorch. As expected, the sample-based methods have the lowest computation time per iteration. This is because they do not need to compute gradients. However, we found that we had to increase the number of iterations in order for them to make progress on the task. Accounting for this, for the quadrotor experiment MPPI and SVMPC are still substantially faster than CSVTO with online trajectory computation times of 0.27s, 0.32s and 0.601s respectively. However, for the manipulator on a surface task the online trajectory computation times are comparable, with MPPI taking 1.41s vs CSVTO’s 1.62s. For the wrench task, the CSVTO is faster than the sample-based methods with 0.732s to generate an online trajectory vs 1.36s for MPPI. We found that CSVTO has a lower computation time than IPOPT for all experiments, often by a factor of more than 2. For instance, for the quadrotor, one iteration of CSVTO takes 60.1ms, while one iteration of IPOPT takes 202ms. In principle IPOPT may terminate early if the trajectory has converged, however within the number of iterations we specified IPOPT did not converge. SVMPC-grad’s

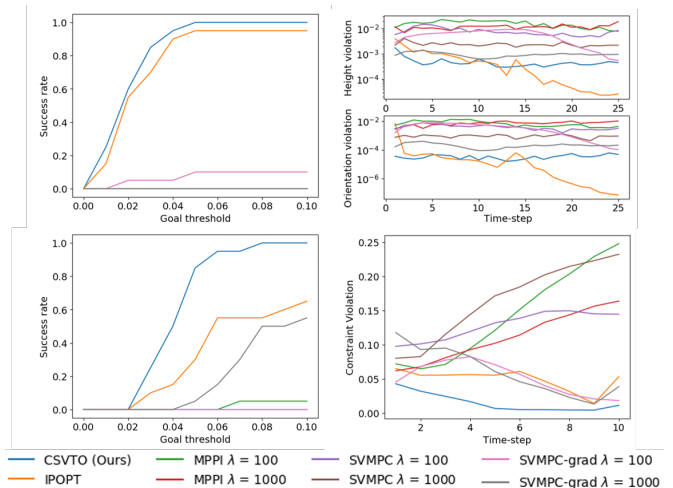


Fig. 6. Results for robot manipulator experiments. Left column shows success rate as we increase the size of the goal region. Right column shows average constraint violation as a function of time. Top) Robot manipulator on a surface experiment. Bottom) Robot manipulating wrench experiment.

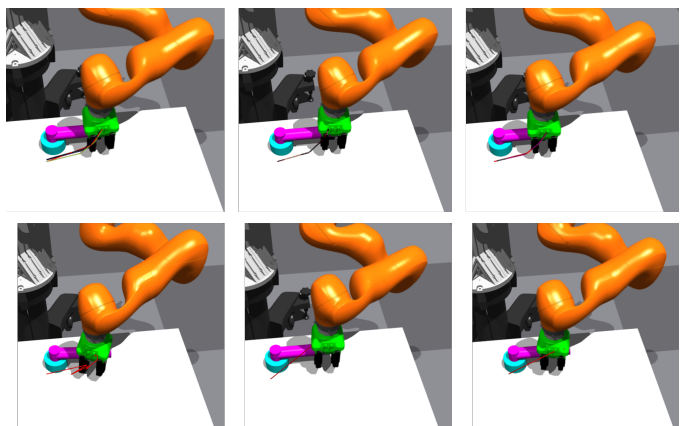


Fig. 7. End effector path visualized for three different initial trajectories generated Top) CSVTO, end-effector path traces an arc around the wrench center to turn the wrench. Bottom) IPOPT, generated trajectories are often poor, exhibiting very large step-sizes and non-smooth trajectories.

computation times were often comparable with CSVTO. While CSVTO requires the computation of the second derivative of the constraints, the cost evaluation of SVMPC-grad requires a loop through the time horizon, slowing down both cost and gradient evaluation. Since CSVTO employs a collocation scheme this is vectorized. Whether CSVTO or SVMPC-grad is faster depends on the relative strength of these two factors.

IX. DISCUSSION

In this section we will discuss some of the advantages of CSVTO over baselines, and then discuss some limitations and

Quadrotor					
Method	Iteration time (ms)	K_{warmup}	Time to initial trajectory (s)	K_{online}	Time to online (s)
CSVTO (Ours)	60.1	100	6.01	10	0.601
IPOPT	202	100	20.2	10	2.02
SVMPC	12.9	250	3.23	25	0.323
SVMPC-grad	80.7	100	8.07	10	0.807
MPPI	10.8	250	2.7	25	0.270
Manipulator on surface					
Method	Iteration time (ms)	K_{warmup}	Time to initial trajectory (s)	K_{online}	Time to online (s)
CSVTO (Ours)	162	100	16.2	10	1.62
IPOPT	281	100	28.1	10	2.81
SVMPC	59.52	250	14.9	25	1.49
SVMPC-grad	114	100	11.4	10	1.14
MPPI	56.5	250	14.1	25	1.41
Manipulator wrench					
Method	Iteration time (ms)	K_{warmup}	Time to initial trajectory (s)	K_{online}	Time to online (s)
CSVTO (Ours)	73.2	100	7.32	10	0.732
IPOPT	139	100	13.9	10	1.39
SVMPC	57.5	250	14.4	25	1.44
SVMPC-grad	157	100	15.7	10	1.57
MPPI	53.4	250	13.6	25	1.36

TABLE II
AVERAGE COMPUTATION TIMES FOR CSVTO AND ALL BASELINE METHODS.

finally highlight areas for future work.

A. Local minima

CSVTO results in diverse constraint-satisfying trajectories. By encouraging diversity through the course of the optimization the algorithm searches the solution space more widely and can result in multi-modal sets of solutions, for example, see Figure 4. We found that this behavior is beneficial for escaping from local minima. This was most clearly demonstrated in the 12DoF Quadrotor experiment. We found that in the case of static and no obstacles, IPOPT was consistently able to get relatively close to the goal, achieving 100% success rate at a goal region of 0.8m. However, it was unable to escape a local minimum in the vicinity of the goal region. This local minimum appears to be induced by the surface constraint, as IPOPT frequently became stuck at a position where it needed to climb in height to reach the goal while satisfying the constraint, incurring a large control cost. In contrast, CSVTO was able to achieve a 100% success with a much smaller goal region of 0.4m.

B. Initialization

CSVTO optimizes a set of trajectories in parallel. Each of these trajectories has a different random initialization, and, as mentioned, the objective encourages trajectory diversity. We find that this approach is effective at making the algorithm more robust to poor initialization. This is most clearly seen in the 7DoF wrench manipulation experiment, shown in Figure 7. This system is highly constrained, and we can see from figure 7 that the trajectories generated by IPOPT can be very low quality when poorly initialized. This is reflected in the success rates, where in our experiments CSVTO succeeds for 20/20 of the trials vs. 13/20 for IPOPT, which was the most competitive baseline.

C. Limitations & Future Work

Our approach does have several limitations which we discuss here. First, our method requires that all constraints

are twice differentiable and uses the second derivative of the constraints to calculate the derivative of the kernel. This is a restrictive assumption, particularly when treating dynamics as a constraint. Many contact-rich robot manipulation tasks exhibit discontinuities that invalidate this assumption.

Second, our approach converts inequality constraints to equality constraints by introducing slack variables. While this is a natural way of incorporating inequality constraints into our method, it results in increasing the number of decision variables by the number of inequality constraints. This is likely to be problematic for long-horizon planning tasks with many inequality constraints. A possible solution would be solving a QP subproblem at every iteration to determine the active inequality constraints as in [46], however, this has the issue that we would need to solve an individual QP subproblem for every particle.

Finally, while our approach decomposes the kernel into a sum of kernels operating on sub-trajectories, each of these kernels is an RBF kernel. While the RBF has attractive properties, such as strict positive-definiteness and smoothness, we believe that exploring task-specific kernels for trajectory optimization is an interesting avenue for future work.

X. CONCLUSION

In this article, we presented Constrained Stein Variational Trajectory Optimization (CSVTO), an algorithm for performing trajectory optimization on a set of trajectories in parallel. To develop CSVTO we formulated constrained trajectory optimization as a Bayesian inference problem, and proposed a constrained Stein Variational Gradient Descent (SVGD) algorithm inspired by O-SVGD [11] for approximating the posterior over trajectories. Our results demonstrate that CSVTO outperforms baselines in challenging highly constrained tasks, such as a 7DoF wrench manipulation task, where CSVTO succeeds in 20/20 trials vs 13/20 for IPOPT. Additionally, our results demonstrate that generating diverse constraint-satisfying trajectories improves robustness to disturbances, such as moving obstacles, as well as robustness to initialization.

REFERENCES

- [1] R. Bonalli, A. Cauligi, A. Bylard, and M. Pavone, “Gusto: Guaranteed sequential trajectory optimization via sequential convex programming,” in *Proc. IEEE Int. Conf. Robot. Autom.*, 2019, pp. 6741–6747.
- [2] J. Schulman, Y. Duan, J. Ho, A. Lee, I. Awwal, H. Bradlow, J. Pan, S. Patil, K. Goldberg, and P. Abbeel, “Motion planning with sequential convex optimization and convex collision checking,” *Int. J. Rob. Res.*, vol. 33, no. 9, pp. 1251–1270, 2014.
- [3] T. A. Howell, B. E. Jackson, and Z. Manchester, “Altro: A fast solver for constrained trajectory optimization,” in *Proc. IEEE/RSJ Int. Conf. Intell. Robots Syst.*, 2019, pp. 7674–7679.
- [4] M. S. Phoon, P. S. Schmitt, and G. V. Wichert, “Constraint-based task specification and trajectory optimization for sequential manipulation,” in *Proc. IEEE/RSJ Int. Conf. Intell. Robots Syst.*, 2022, pp. 197–202.
- [5] C. Brasseur, A. Sherikov, C. Collette, D. Dimitrov, and P.-B. Wieber, “A robust linear mpc approach to online generation of 3d biped walking motion,” in *Proc. 15th IEEE-RAS Int. Conf. Humanoid Robots*, 2015, p. 595–601.
- [6] A. Lambert and B. Boots, “Entropy regularized motion planning via stein variational inference,” 2021, arxiv.2107.05146.
- [7] D. M. Blei, A. Kucukelbir, and J. D. McAuliffe, “Variational inference: A review for statisticians,” *J. Am. Stat. Assoc.*, vol. 112, no. 518, pp. 859–877, 2017.
- [8] H. Yu and Y. Chen, “A gaussian variational inference approach to motion planning,” *IEEE Robot. Autom. Lett.*, vol. 8, no. 5, pp. 2518–2525, 2023.
- [9] M. Mukadam, X. Yan, and B. Boots, “Gaussian process motion planning,” in *Proc. IEEE Int. Conf. Robot. Autom.*, 2016, pp. 9–15.
- [10] A. Lambert, A. Fishman, D. Fox, B. Boots, and F. Ramos, “Stein variational model predictive control,” in *Proc. Conf. Robot Learn.*, 2020.
- [11] R. Zhang, Q. Liu, and X. Tong, “Sampling in constrained domains with orthogonal-space variational gradient descent,” *Proc. Int. Conf. Neural Information Processing Systems*, vol. 35, pp. 37 108–37 120, 2022.
- [12] A. Wächter and L. T. Biegler, “On the implementation of an interior-point filter line-search algorithm for large-scale nonlinear programming,” *Math. Program.*, vol. 106, no. 1, p. 25–57, March 2006.
- [13] T. Apgar, P. Clary, K. Green, A. Fern, and J. W. Hurst, “Fast online trajectory optimization for the bipedal robot cassie,” in *Robot.: Sci. Syst.*, 2018.
- [14] P. E. Gill, W. Murray, and M. A. Saunders, “Snopt: An sqp algorithm for large-scale constrained optimization,” *SIAM Rev.*, vol. 47, no. 1, p. 99–131, Jan 2005.
- [15] J. Hauser and A. Saccon, “A barrier function method for the optimization of trajectory functionals with constraints,” in *IEEE 45th Conf. Decision and Control*, 2006, pp. 864–869.
- [16] R. Ni, T. Schneider, D. Panozzo, Z. Pan, and X. Gao, “Robust & asymptotically locally optimal uav-trajectory generation based on spline subdivision,” in *Proc. IEEE Int. Conf. Robot. Autom.*, 2021, pp. 7715–7721.
- [17] D. Q. Mayne, “A second-order gradient method for determining optimal trajectories of non-linear discrete-time systems,” *Int. J. Control*, vol. 3, pp. 85–95, 1966.
- [18] W. Li and E. Todorov, “Iterative linear quadratic regulator design for nonlinear biological movement systems,” in *Proc. IEEE Int. Conf. Inform. Control. Autom. Robot.*, 2004.
- [19] M. Gifthalder and J. Buchli, “A projection approach to equality constrained iterative linear quadratic optimal control,” in *Proc. 17th IEEE-RAS Int. Conf. Humanoid Robotics*, 2017, p. 61–66.
- [20] Z. Xie, C. K. Liu, and K. Hauser, “Differential dynamic programming with nonlinear constraints,” in *Proc. IEEE Int. Conf. Robot. Autom.*, 2017, pp. 695–702.
- [21] O. Von Stryk and R. Bulirsch, “Direct and indirect methods for trajectory optimization,” *Annals of operations research*, vol. 37, pp. 357–373, 1992.
- [22] D. Berenson, S. Srinivasa, and J. Kuffner, “Task space regions: A framework for pose-constrained manipulation planning,” *Int. J. Rob. Res.*, vol. 30, no. 12, pp. 1435–1460, 2011.
- [23] J. Mirabel, S. Tonneau, P. Fernbach, A.-K. Seppälä, M. Campana, N. Mansard, and F. Lamiroux, “Hpp: A new software for constrained motion planning,” in *Proc. IEEE/RSJ Int. Conf. Intell. Robots Syst.*, 2016, pp. 383–389.
- [24] L. Jaillet and J. M. Porta, “Path planning under kinematic constraints by rapidly exploring manifolds,” *IEEE Trans. Robot.*, vol. 29, no. 1, pp. 105–117, 2013.
- [25] J. M. Porta, L. Jaillet, and O. Bohigas, “Randomized path planning on manifolds based on higher-dimensional continuation,” *Int. J. Rob. Res.*, vol. 31, no. 2, pp. 201–215, 2012.
- [26] M. Mukadam, J. Dong, X. Yan, F. Dellaert, and B. Boots, “Continuous-time gaussian process motion planning via probabilistic inference,” *Int. J. Rob. Res.*, vol. 37, no. 11, pp. 1319–1340, 2018.
- [27] M. Toussaint and A. Storkey, “Probabilistic inference for solving discrete and continuous state markov decision processes,” in *Proc. Int. Conf. Mach. Learn.*, 2006, p. 945–952.
- [28] K. Rawlik, M. Toussaint, and S. Vijayakumar, “On stochastic optimal control and reinforcement learning by approximate inference,” in *Robot.: Sci. Syst.*, 2013.
- [29] J. Watson, H. Abdulsamad, and J. Peters, “Stochastic optimal control as approximate input inference,” in *Proc. Conf. Robot Learn.*, vol. 100, 2020, pp. 697–716.
- [30] G. Williams, P. Drews, B. Goldfain, J. M. Rehg, and E. A. Theodorou, “Information-theoretic model predictive control: Theory and applications to autonomous driving,” *IEEE Trans. Robot.*, vol. 34, no. 6, p. 1603–1622, Dec 2018.
- [31] M. Kobilarov, “Cross-entropy motion planning,” *Int. J. Rob. Res.*, vol. 31, no. 7, pp. 855–871, 2012.
- [32] Z. Wang, O. So, J. Gibson, B. Vlahov, M. Gandhi, G.-H. Liu, and E. Theodorou, “Variational Inference MPC using Tsallis Divergence,” in *Robot.: Sci. Syst.*, 2021.
- [33] J. Watson and J. Peters, “Inferring smooth control: Monte carlo posterior policy iteration with gaussian processes,” in *Proc. Conf. Robot. Learn.*, 2023, pp. 67–79.
- [34] T. Power and D. Berenson, “Variational inference mpc using normalizing flows and out-of-distribution projection,” in *Robot.: Sci. Syst.*, 2022.
- [35] J. Sacks and B. Boots, “Learning sampling distributions for model predictive control,” in *Proc. Conf. Robot. Learn.*, 2023, pp. 1733–1742.
- [36] Q. Liu and D. Wang, “Stein variational gradient descent: A general purpose bayesian inference algorithm,” in *Proc. Int. Conf. Neural Information Processing Systems*, 2016, p. 2378–2386.
- [37] L. Barcelos, A. Lambert, R. Oliveira, P. Borges, B. Boots, and F. Ramos, “Dual Online Stein Variational Inference for Control and Dynamics,” in *Robot.: Sci. Syst.*, 2021.
- [38] A. Lambert, B. Hou, R. Scalise, S. S. Srinivasa, and B. Boots, “Stein variational probabilistic roadmaps,” in *Proc. IEEE Int. Conf. Robot. Autom.*, 2022, pp. 11 094–11 101.
- [39] I. M. Balci, E. Bakolas, B. Vlahov, and E. A. Theodorou, “Constrained covariance steering based tube-mppi,” in *2022 American Control Conference (ACC)*, 2022, pp. 4197–4202.
- [40] T. Osa, “Multimodal trajectory optimization for motion planning,” *Int. J. Rob. Res.*, vol. 39, no. 8, pp. 983–1001, 2020.
- [41] M. Zucker, N. Ratliff, A. D. Dragan, M. Pivtoraiko, M. Klingensmith, C. M. Dellin, J. A. Bagnell, and S. S. Srinivasa, “Chomp: Covariant hamiltonian optimization for motion planning,” *Int. J. Rob. Res.*, vol. 32, no. 9-10, pp. 1164–1193, 2013.
- [42] H. Yamashita, “A differential equation approach to nonlinear programming,” *Math. Program.*, vol. 18, no. 1, pp. 155–168, 1980.
- [43] J. Schropp and I. Singer, “A dynamical systems approach to constrained minimization,” *Numer. Funct. Anal. Optim.*, vol. 21, no. 3-4, pp. 537–551, 2000.
- [44] V. Shikhman and O. Stein, “Constrained optimization: projected gradient flows,” *J. Optim. Theory. Appl.*, vol. 140, no. 1, pp. 117–130, 2009.
- [45] H. T. Jongen and O. Stein, “Constrained global optimization: Adaptive gradient flows,” in *Frontiers in Global Optimization*, C. A. Floudas and P. Pardalos, Eds., 2004, p. 223–236.
- [46] Feppon, F., Allaire, G., and Dapogny, C., “Null space gradient flows for constrained optimization with applications to shape optimization,” *ESAIM: COCV*, vol. 26, p. 90, 2020.
- [47] Q. Liu, “Stein variational gradient descent as gradient flow,” in *Proc. Int. Conf. Neural Information Processing Systems*, I. Guyon, U. V. Luxburg, S. Bengio, H. Wallach, R. Fergus, S. Vishwanathan, and R. Garnett, Eds., 2017.
- [48] M. Toussaint, “Robot trajectory optimization using approximate inference,” in *Proc. Int. Conf. Mach. Learn.*, 2009, p. 1049–1056.
- [49] M. Okada and T. Taniguchi, “Variational inference mpc for bayesian model-based reinforcement learning,” in *Proc. Conf. Robot Learn.*, 2020, pp. 258–272.
- [50] J. Urain, A. T. Le, A. Lambert, G. Chalvatzaki, B. Boots, and J. Peters, “Learning implicit priors for motion optimization,” in *Proc. IEEE/RSJ Int. Conf. Intell. Robots Syst.*, 2022, pp. 7672–7679.
- [51] H. Attias, “Planning by probabilistic inference,” in *Proc. 9th Int. Workshop on Artificial Intelligence and Statistics*, 2003, pp. 9–16.
- [52] Q. Liu, J. D. Lee, and M. Jordan, “A kernelized stein discrepancy for goodness-of-fit tests,” in *Proc. Int. Conf. Mach. Learn.*, 2016, p. 276–284.

- [53] D. Wang, Z. Tang, C. Bajaj, and Q. Liu, “Stein variational gradient descent with matrix-valued kernels,” *Proc. Int. Conf. Neural Information Processing Systems*, vol. 32, 2019.
- [54] E. H. Fukuda and M. Fukushima, “A note on the squared slack variables technique for nonlinear optimization,” *J. Oper. Res. Soc. Japan*, vol. 60, no. 3, pp. 262–270, 2017.
- [55] F. D’Angelo and V. Fortuin, “Annealed stein variational gradient descent,” 2021, arxiv.2101.09815.
- [56] J. D. Hol, T. B. Schon, and F. Gustafsson, “On resampling algorithms for particle filters,” in *2006 IEEE Nonlinear Statistical Signal Processing Workshop*, 2006, pp. 79–82.
- [57] V. Makoviychuk, L. Wawrzyniak, Y. Guo, M. Lu, K. Storey, M. Macklin, D. Hoeller, N. Rudin, A. Allshire, A. Handa, and G. State, “Isaac gym: High performance gpu-based physics simulation for robot learning,” 2021, arxiv.2108.10470.
- [58] A. Paszke, S. Gross, F. Massa, A. Lerer, J. Bradbury, G. Chanan, T. Killeen, Z. Lin, N. Gimelshein, L. Antiga, A. Desmaison, A. Köpf, E. Yang, Z. DeVito, M. Raison, A. Tejani, S. Chilamkurthy, B. Steiner, L. Fang, J. Bai, and S. Chintala, *PyTorch: An Imperative Style, High-Performance Deep Learning Library*, 2019.
- [59] P. R. Amestoy, A. Guermouche, J.-Y. L’Excellent, and S. Pralet, “Hybrid scheduling for the parallel solution of linear systems,” *Parallel Computing*, vol. 32, no. 2, pp. 136–156, 2006.
- [60] F. Sabatino, “Quadrotor control: modeling, nonlinear control design, and simulation,” Master’s thesis, KTH Royal Institute of Technology, 2015.